Monte Carlo Simulations of 2D Ising Model

Chemistry 444, Computation Final Project

Department of Materials Science and Engineering

Northwestern University, Evanston IL

Brandon N. Onusaitis

Preface

The derivations shown herein were adapted from Frenkel & Smit and Allen & Tildesley.[1,2]

Statistical Mechanics Basis for Free Energy Measurements

The free energy of a system in the canonical ensemble depends on the partition function and the fixed temperature through the following relation:

$$F = -k_b T \ln[Q(N,V,T] \tag{1}$$

Since free energies are not absolute, only relative free energies can be measured in experiment or simulation. The free energy change between two states, denoted 1 and 2, is a function of their respective partition functions:

$$\Delta F = -k_b T \ln\left[\frac{\int dM^N e^{-\beta E_2(M^N)}}{\int dM^N e^{-\beta E_1(M^N)}}\right] \tag{2}$$

where M^N is the dimension of the configuration space, and E_1 and E_2 are the energies of systems 1 and 2, respectively. Given the high-dimensional space of the partition functions and the Boltzmann sampling employed in traditional metropolis algorithm, there is a need to estimate the partition functions through biased sampling.

To relate the free energy to a measurable quantity in simulation, a relationship between the probability of finding a potential energy difference between system 2 and system 1 must be articulated. The probability, $P_2(\Delta E)$, of one such potential energy difference can be expressed as:

$$P_2(\Delta E) = \frac{\int dM^N e^{-\beta E_2(M^N)} \delta[E_2(M^N) - (E_1(M^N) + \Delta E(M^N)]}{Q_2(N,V,T)} \tag{3}$$

where the delta function ensures the energy of system 2 is evaluated under the ΔE constraint. Specifically, the delta function yields the correct Boltzmann factor in terms of system 2's energy. Rewriting the Boltzmann factor for system 2's energy, we have:

$$e^{-\beta E_2(M^N)} = e^{-\beta\left(E_2(M^N) - E_1(M^N)\right)} e^{-\beta E_1(M^N)} = e^{-\beta \Delta E(M^N)} e^{-\beta E_1(M^N)} \tag{4}$$

By rewriting Equation (3) in terms of a ratio of partition functions, the expression becomes:

$$P_2(\Delta E) = \frac{\int dM^N e^{-\beta \Delta E(M^N)} e^{-\beta E_1(M^N)} \delta[E_2(M^N) - (E_1(M^N) + \Delta E(M^N)]}{Q_2(N,V,T)} \tag{5}$$

$$P_2(\Delta E) = \frac{e^{-\beta \Delta E(M^N)}}{Q_2(N,V,T)} \int dM^N e^{-\beta E_1(M^N)} \delta[E_2(M^N) - (E_1(M^N) + \Delta E(M^N)] \tag{6}$$

Based on our definition shown in Equation (3), the integral can be exchanged with the probability of system 1 multiplied by its partition function:

$$P_2(\Delta E) = \frac{e^{-\beta \Delta E(M^N)}}{Q_2(N,V,T)} Q_1(N,V,T) P_1(\Delta E) \tag{7}$$

This formulation facilitates the connection between the probability of potential energy differences and partition functions, which provides a means to leverage biased sampling in monte carlo (MC) simulations. It is important to clarify, that $P_2(\Delta E)$ indicates the probability of finding an energy difference between system 2 and 1 while Boltzmann sampling system 2—the same can be said for $P_1(\Delta E)$. Moreover, taking the natural log of Equation (7) and using the definition shown in Equation (2) we get an expression relating the probabilities and the free energy:

$$\ln P_2(\Delta E) = \ln \frac{Q_1(N,V,T)}{Q_2(N,V,T)} - \beta \Delta E + \ln P_1(\Delta E) \tag{8}$$

$$\ln P_2(\Delta E) = \beta \ln \Delta F - \beta \Delta E + \ln P_1(\Delta E) \tag{9}$$

In principle, the free energy can be determined by employing Equation (9) through Metropolis MC simulations with Boltzmann sampling for both systems 1 and 2. That is, the disparity separating each systems' histogram is directly related to the free energy difference between them. However, this method falls short when attempting to capture the free energies between systems separated by a large energy barrier—a scenario where Boltzmann proves inadequate. As a remedy, the established practice is conducting MC simulation at intermediate energy separations through a biased potential. Subsequently, the histograms are integrated, and the probabilities are written as a linear combination that sums to the unbiased distribution function value. While I won't include the derivation of this method, I will present the final outcome, as described in Frenkel and Smit.[1]

$$P_0^{est} = \frac{\sum_i^S H_i(M)}{\sum_{i=1}^S C_i \frac{Q_0(N,V,T)}{Q_i(N,V,T)} e^{-\beta V_{bias,i}}} \tag{10}$$

$$Q_i(N,V,T) = \int dM^N e^{-\beta V_{bias,i}} \frac{\sum_{j=1}^n H_j(M)}{\sum_{k=1}^n C_k \frac{e^{-\beta V_{bias,k}}}{Q_k(N,V,T)}} \tag{11}$$

Equation (10) gives the target probability distribution, which is crucial to estimating the Landau free energy. Together, these equations constitute the self-consistent histogram method, also known as Weighted Histogram Analysis Method (WHAM). Solving Equations (10) and (11) involves an iterative process, usually through fixed-point direct iteration method.[3] However, in this work a recursion relation will be derived, as discussed in Frenkel and Smit. The derivation of the recursion relation demands two key assumptions: the use of an infinite square well biasing potential and a window only overlaps with its adjacent window functions. These assumptions will be addressed subsequent to our derivation of the recursion relation. Let our window function be defined as,

$$V_{bias,i} = \begin{cases} \infty & M_i < M_i^{min} \\ 0 & M_i^{min} < M_i < M_i^{max} \\ \infty & M_i > M_i^{max} \end{cases} \tag{12}$$

where M_i is the magnetization (order parameter) over which the biasing potential samples. Ideally, the biasing potential, $V_{bias,i}$ is chosen such that it overlaps exclusively with the adjacent windows, as formulated in Equation (13) and shown in Figure 1.

$$\begin{aligned} M_{i-2}^{max} < M_i^{min} < M_{i-1}^{max} \\ M_{i+2}^{min} > M_i^{max} > M_{i+1}^{\min} \end{aligned} \tag{13}$$

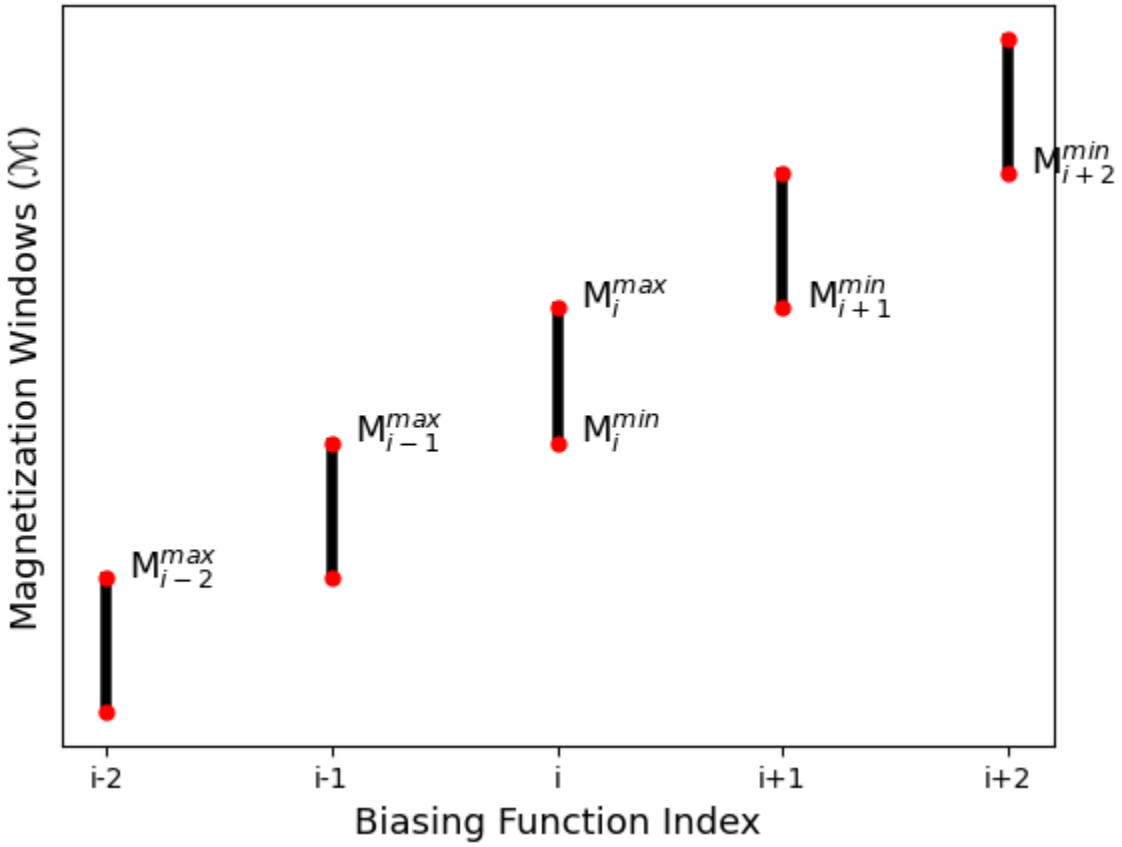

Figure 1: Window function with magnetization range on the ordinate and window function index on the abscissa. This illustrates the ideal scenario where only adjacent windows overlap over a specified range of magnetizations.

The recursive relation can be derived for the biasing function in Equation (12) and by evaluating Equation (11). In Equation (11), H_j is histogram j and C_k is the number of points falling within histogram j. Thus,

$$P_j = \frac{H_j}{C_k} \qquad \forall j,k : \delta_{jk} = \begin{cases} 1 & j = k \\ 0 & j \neq k \end{cases} \tag{14}$$

substituting Equation (14) into Equation (11) yields,

$$Q_i(N,V,T) = \int dM e^{-\beta V_{bias,i}} \frac{\sum_i^n P_i(M)}{\sum_i^n \frac{e^{-\beta V_{bias,i}}}{Q_i}} \tag{15}$$

where P_i is the ith simulation's probability density. When evaluating the partition function Q_i, we perform integration over all space. However, the Boltzmann factor of the biasing function alters the bound, which renders the integrand zero for all magnetization values outside the interval $[M_i^{min}, M_i^{max}]$.

$$Q_i(N,V,T) = \int_{-\infty}^{+\infty} dM e^{-\beta V_{bias,i}} \frac{\sum_i^n P_i(M)}{\sum_i^n \frac{e^{-\beta V_{bias,i}}}{Q_i}} = \int_{M_i^{\min}}^{M_i^{max}} dM \frac{\sum_i^n P_i(M)}{\sum_i^n \frac{e^{-\beta V_{bias,i}}}{Q_i}} \tag{16}$$

The integral on the right-hand side of Equation (16) can be decomposed into the sum of integrals over three continuous intervals, collectively covering the entire domain, $[M_i^{min}, M_i^{max}]$.

$$\int_{M_i^{\min}}^{M_i^{max}} dM \frac{\sum_i^n P_i(M)}{\sum_i^n \frac{e^{-\beta V_{bias,i}}}{Q_i}} = \int_{M_i^{\min}}^{M_{i-1}^{max}} dM + \int_{M_{i-1}^{\max}}^{M_{i+1}^{min}} dM + \int_{M_{i+1}^{\min}}^{M_i^{max}} dM \frac{\sum_i^n P_i(M)}{\sum_i^n \frac{e^{-\beta V_{bias,i}}}{Q_i}} \tag{17}$$

Equation (17) is much simpler to evaluate since many terms will cancel out due to the three sub intervals. For example, in the numerator, the summation of probabilities across each window ensures only two terms survive in each integral. This is a consequence of the probability being zero outside the domain encompassed by the integration bounds. Therefore,

$$\int_{M_{i-1}^{\max}}^{M_{i+1}^{min}} dM \sum_i^n P_i(M) = \int_{M_{i-1}^{\max}}^{M_{i+1}^{min}} dM \; P_1 + \cdots + P_{i-1} + P_i + P_{i+1} + \cdots + P_n = \int_{M_{i-1}^{\max}}^{M_{i+1}^{min}} dM \; P_{i-1} + P_{i+1} \tag{18}$$

where this same argument holds true for the remaining two integrals. The subsequent task is to evaluate the denominator of each integral in Equation (17). By expanding the sum of each biased probability and evaluating each window function both within and outside its bounds, it becomes evident only two non-trivial terms persist:

$$\int_{M_{i-1}^{\max}}^{M_{i+1}^{min}} dM \frac{1}{\sum_i^n \frac{e^{-\beta V_{bias,i}}}{Q_i}} =$$

$$\int_{M_{i-1}^{\max}}^{M_{i+1}^{min}} dM \frac{1}{\frac{e^{-\beta V_{bias,1}}}{Q_1} + \cdots + \frac{e^{-\beta V_{bias,i-1}}}{Q_{i-1}} + \frac{e^{-\beta V_{bias,i}}}{Q_i} + \frac{e^{-\beta V_{bias,i+1}}}{Q_{i+1}} + \cdots + \frac{e^{-\beta V_{bias,n}}}{Q_n}} =$$

$$\int_{M_{i-1}^{\max}}^{M_{i+1}^{min}} dM \frac{1}{0 + \cdots + \frac{e^{-\beta 0}}{Q_{i-1}} + 0 + \frac{e^{-\beta 0}}{Q_{i+1}} + \cdots + 0} = \int_{M_{i-1}^{\max}}^{M_{i+1}^{min}} dM \frac{1}{\frac{1}{Q_{i-1}} + \frac{1}{Q_{i+1}}} \tag{19}$$

Substituting the results from Equations (18) and (19) into Equation (17), the following expression is obtained:

$$Q_i(N,V,T) = \int_{M_i^{\min}}^{M_{i-1}^{max}} dM \frac{Q_{i-1}Q_i[P_i(M)+P_{i-1}(M)]}{Q_{i-1}+Q_i} + \int_{M_{i-1}^{\max}}^{M_{i+1}^{min}} dM \frac{Q_{i+1}Q_{i-1}[P_{i+1}(M)+P_{i-1}(M)]}{Q_{i-1}+Q_{i+1}} + \int_{M_{i+1}^{\min}}^{M_i^{max}} dM \frac{Q_{i+1}Q_i[P_{i+1}(M)+P_i(M)]}{Q_i+Q_{i+1}} \quad (20)$$

From Equation (20), the recursion relation can be derived, and for the sake of time I will exclude the algebra required to go from Equation (20) to the expressions shown in Equations (21) and (22).

$$Q_{i+1} = -\frac{Q_iQ_{i-1}A_i + (Q_iQ_{i-1}+Q_iQ_i)B_i}{Q_{i-1}A_i + (Q_{i-1}+Q_i)B_i + (Q_{i-1}+Q_i)C_i} \quad (21)$$

$$A_i, B_i, C_i = \begin{cases} A_i = \int_{M_i^{\min}}^{M_{i-1}^{max}} dM[P_i(M)+P_{i-1}(M)] \\ B_i = -1 + \int_{M_{i-1}^{\max}}^{M_{i+1}^{min}} dM\, P_i(M) \\ C_i = \int_{M_{i+1}^{\min}}^{M_i^{max}} dM[P_{i+1}(M)+P_i(M)] \end{cases} \quad (22)$$

Equation (21) represents a recursion relation which is used to generate successive partition functions. These partition functions are essential to obtaining the distribution illustrated in equation 10, and, subsequently, for evaluating the Landau free energy. If Q_1 is set 1 and the first window exclusively overlaps with window 2 (A = 0), then Equation (21) simplifies to Equation (23):

$$Q_2 = -\frac{B_1}{B_1+C_1} \quad (23)$$

The second window's partition function, Q_2, can then be used to compute Q_3 and so forth. This methodology was applied in this project and gives an initial first estimate for the probability density, and hence the free energy.

Methods

The umbrella potential used in the biased MC simulations was a conventional harmonic function centered about magnetization values of interest. Its form is shown in Equation (24):

$$V_{bias,i} = k_M(M-M_0)^2 \quad (24)$$

The biased potential was added to the Boltzmann sampling factor giving the following criteria for acceptance of a MC move:

$$P_{acceptance} = \min\left(1, e^{-\beta(\Delta E_{ising}+k_M(M-M_0)^2)}\right)$$

A spring constant on the order of 10^3 k_BT was required to adequately sample the unfavorable states when T approached the critical temperature, T_c. The simulations were performed with zero magnetic field (h = 0), making the Ising Hamiltonian reduce to the sum of the coupling terms. One hundred MC simulations with 4×10^4 MC steps per simulation were performed for temperatures below T_C, around T_c, and above T_c. This corresponded $\beta > 0.44$, $\beta = 0.44$, $\beta < 0.44$, respectively.

Results

In this project, biased sampling was successfully achieved through an umbrella potential. The successful sampling is illustrated in Figure 2, where the mean is approximately centered around the biasing potentials' minimum magnetization per site.

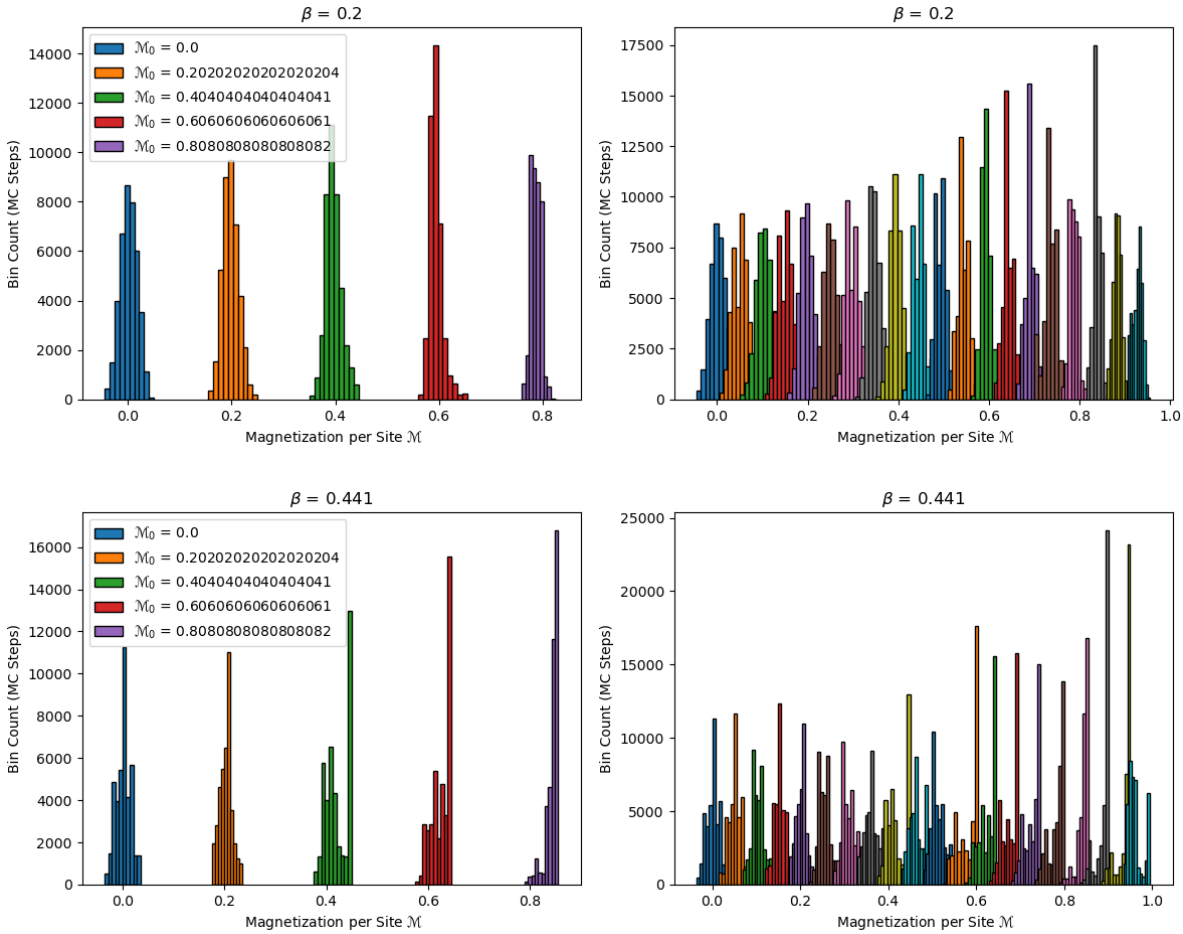

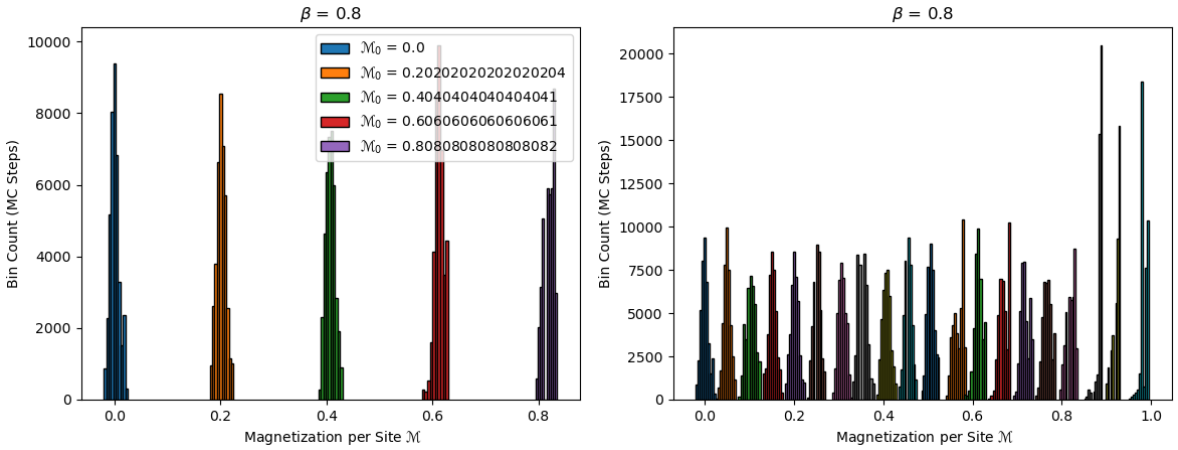

Figure 2: Non-normalized sampling results from biased MC simulations. On the left-hand side are samples from 5 windows, each collected with a target magnetization. The right-hand side displays 20 out of the 100 windows sampled. These were performed at a variety of temperatures.

It is worth noting that each configuration started with a random configuration of approximately zero net magnetization per site. Achieving high quality sampling was relatively straightforward for $\beta < \beta_c$, specifically at β= 0.2, since the initial configuration was already near the free energy minimum. However, challenges arose when attempting to attain quality biased sampling for β near or above the critical point. Precise tuning of both the spring constant and the number of windows was crucial to achieve an adequate sampling profile, as shown Figure 2. If the spring constant was too high, no moves would be accepted, leading the system to be perpetually trapped in a high-energy state. If the spring constant was too low, the harmonic potential would fail to restrain the system to its prescribed window, resulting in poor sampling of the domain. Therefore, attaining these samples required a considerable amount of trial and error.

Another key attribute that contributed to successful sampling was utilizing the ending configuration of one MC simulation as the starting configuration for the adjacent window. This approach ensured the system was sufficiently close, allowing MC moves to guide it towards the harmonic well. Otherwise, if a spin configuration was energetically to distant, no moves would be accepted, regardless if they were favorable.

The free energy trends were estimated by computing the probability densities at various magnetizations using the data from the overlapping histograms. This is synonymous with computing the numerator in Equation (10), which is one of the two equations for the Self-Consistent Histogram Method. The free energy trends are illustrated in Figures 3,4, and 5, and corroborated our predictions from problem set 8.

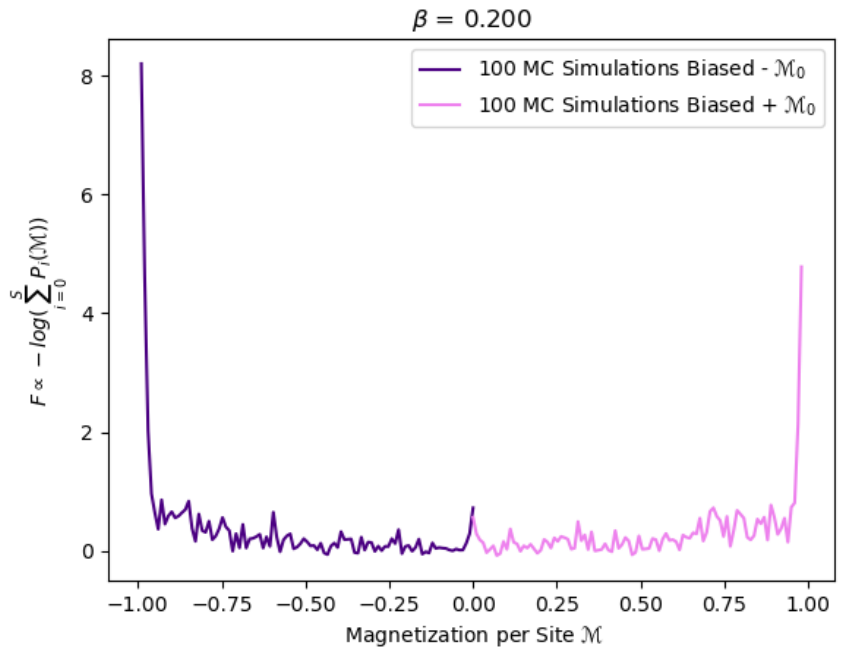

Figure 3: Un-weighted probability density profile as a function of magnetization per site for a temperature greater than the critical temperature. A large, flat polynomial trend with only one apparent minimum is observed.

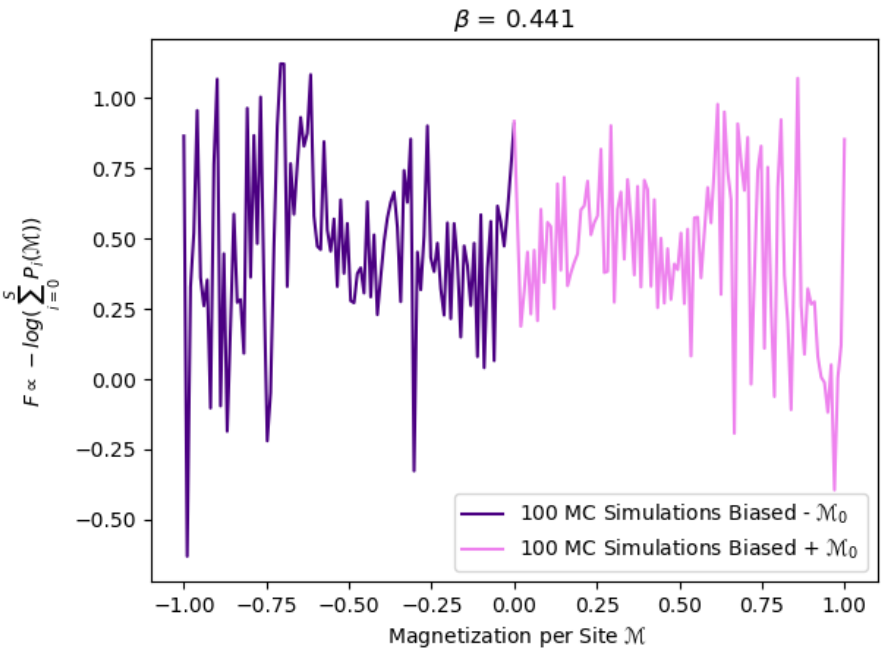

Figure 4: Un-weighted probability density profile as a function of magnetization per site for a temperature near the critical temperature. Sampling across the spectrum with significant variance is observed.

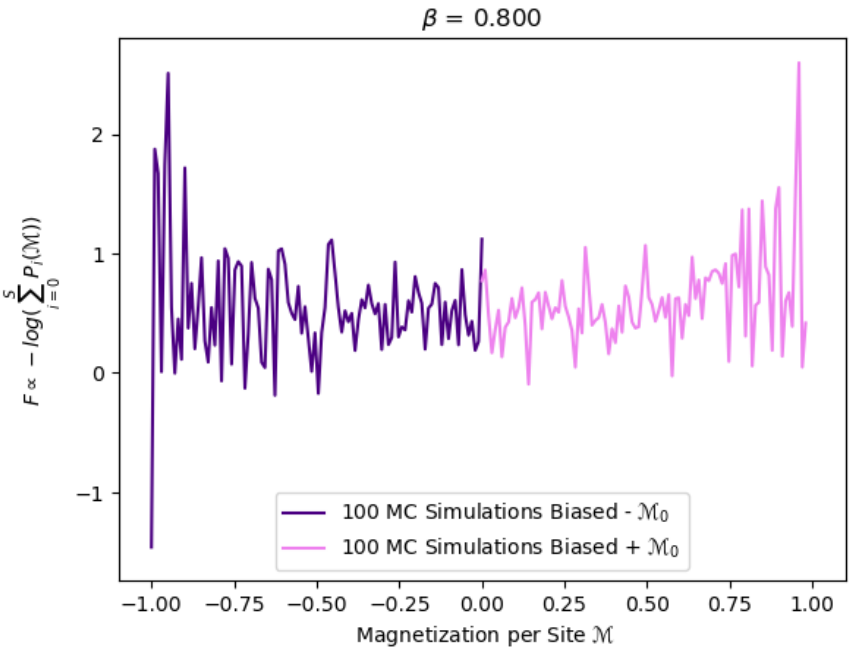

Figure 5: Un-weighted probability density profile as a function of magnetization per site for a temperature below the critical temperature. Sampling across the spectrum with significant variance is observed.

Figure 3 resembles a polynomial with a single flat minimum. This captures the critical point where the Ising model transitions from a phase segregated state, $T < T_C$, to a completely mixed state—$T > T_C$. Figures 4 and 5 both show significant variance across magnetization probabilities. This is to be expected because sampling at lower temperatures becomes increasingly difficult, due to the Ising model's propensity to form a magnetization per site of ±1. Qualitatively, it is interesting to see the fluctuations away from the critical temperature reduce when comparing Figure 4 and Figure 5.

It was expected that below T_C, a free energy profile with two minima at ±1 would be observed. However, due to time constraints, the correct weighting of each histogram's contribution could not be calculated. It is worth including the results from problem set 8's MC simulations, since it provided a guide to this study. From Figure 6, which was obtained from problem set 8, the proper temperature values and spin states could be sampled to get quality data for free energy estimates.

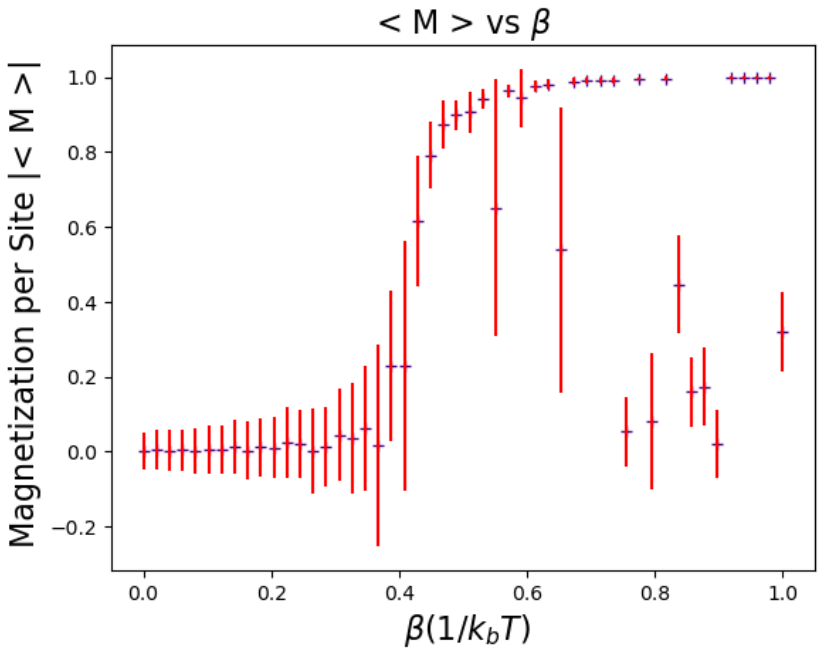

Figure 6: Problem Set 8 MC simulations showing the temperature dependence of the magnetization per site.

Conclusion

While the free energy was not successfully measured, quality preliminary data with promising trends was observed. Additionally, a complete derivation of the recursive relation, shown in Frenkel & Smit, was adapted to the 2D Ising problem using infinite square well window functions. It is hypothesized that the recursion relation, shown in Equation (21), could be used for the umbrella potentials since in the limit of large spring constant, the harmonic function approaches hardcore walls with vanishing width.

References

(1) D. Frenkel, B. Smit, Understanding Molecular Simulation, 2001
(2) M.P. Allen, D.J. Tildesley, Computer Simulation of Liquids, 2017
(3) F. Zhu, G. Hummer, *J Comput Chem.,* 2012